ISSN (print): 1698-6180. ISSN (online): 1886-7995
www.ucm.es/info/estratig/journal.htm

Journal of Iberian Geology 33 (1) 2007: 5-16

Journal of Iberian Geology
AN INTERNATIONAL PUBLICATION OF EARTH SCIENCES

Metamorphic P-T conditions of Late Jurassic rhyolites in the Magallanes fold and thrust belt, Patagonian Andes, Chile

Condiciones P-T de metamorfismo de riolitas del Jurásico Superior en el cinturón de pliegues y mantos de Magallanes, Andes Patagónicos, Chile.

F. Hervé[1], H.-J. Massonne[2], M. Calderón[1], T. Theye[2]

[1]*Departamento de Geología, Universidad de Chile, Casilla 13518, Correo 21. Santiago, Chile*
e-mail: fherve@cec.uchile.cl; caldera@esfera.cl
[2]*Institut für Mineralogie, Universität Stuttgart, 18 Azenbergstrasse, Stuttgart, Germany*
e-mail: h-j.massonne@mineralogie.uni-stuttgart.de; thomas.theye@mineralogie.uni-stuttgart.de

Received: 25/02/06 / Accepted: 10/11/06

Abstract

Foliated meta-rhyolites of the Late Jurassic Tobífera Formation, form two thrust slices in the Patagonian Andes fold and thrust belt. They display a penetrative mylonitic foliation which has been developed at a regional scale. Except for quartz porphyroclasts, most of the mineral assemblage present in the rocks is of metamorphic origin. The synkinematic minerals in the strain shadows are similar in composition to those in the matrix. The metamorphic mineralogy indicates a metamorphic evolution ranging between 3 kbar (ca. 250°C) and close to 7 kbar (ca.350°C), and the synkinematic growth of the minerals suggests that they formed during the Early to middle Cretaceous compressional phase in the area, which possibly involved west directed subduction of the quasi oceanic floor that underlies the Tobífera Formation.

Keywords: Metamorphism, Tobífera Formation, Patagonian Andes, Chile.

Resumen

Meta-riolitas foliadas de la Formación Tobífera (Jurásico Superior) forman dos escamas tectónicas en el cinturón de pliegues y mantos de los Andes Patagónicos. Exhiben una foliación milonítica penetrativa desarrollada a escala regional. Exceptuando a porfiroclastos de cuarzo, la mayor parte de la asociación mineral es de origen metamórfico. Los minerales sincinemáticos, en las sombras de presión, son similares en composición a aquellos de la matriz. La mineralogía metamórfica sugiere una evolución entre unos 3 kbar (aprox. 250 ºC) y unos 7 kbar (aprox. 350 ºC). La naturaleza sincinemática de los minerales permite correlacionarlos con una fase compresional del Cretácico Inferior a medio en la región, que probablemente involucró una subducción dirigida hacia el oeste del sustrato cuasi-oceánico sobre el que se depositó la Formación Tobífera.

Palabras clave: Metamorfismo, Formación Tobífera, Andes Patagónicos, Chile.

1. Introduction

The Tobífera Formation is a Late Jurassic unit of the Magallanes basin in southern South America. It is mainly composed of siliceous volcanic rocks, including rhyolites, tuffs, and ignimbrites, with minor intercalated basalts and clastic sedimentary rocks. The igneous rocks are interpreted to be the product of crustal anatexis (Pankhurst and Rapela, 1995) which took place during widespread extensional events preceding the dismembering of

the Pangea supercontinent and, thus, the opening of the Atlantic Ocean. The Tobífera Formation also crops out in the thrust and fold belt of the Patagonian Andes which limits the Magallanes basin to the west. Here it is mainly composed of foliated metarhyolites and metatuffs, which exhibit one main foliation parallel to the orographic trend of the mountain belt.

The only previous studies about the metamorphic conditions attained by the metarhyolites in the area has been done by Galaz (2005) and Galaz *et al*. (2005) who studied these rocks at Cordillera Riesco, in the southeastern corner of the geological map shown in Figure 1. In this paper we report the mineral associations developed during the metamorphic and deformational event which foliated and almost completely reequilibrated the mineralogy of the Tobífera rocks at the northern part of Fiordo Peel (Fig. 1). From there we deduce the P-T conditions of their metamorphism. Subsequently, we evaluate the geological implications of these results in the evolution of the Patagonian Andes.

2. Field Geology

As shown in figure 1, metarhyolitic rocks of the Tobífera Formation form two elongated bodies which correspond to thrust sheets of the inner Patagonian fold and thrust belt. They are thrust over Early Cretaceous sediments to the east, and are in turn thrust over by granitic and Paleozoic rocks from the west. In outcrop, this unit is spatially related to the Sarmiento ophiolite which developed penecontemporaneously to the Tobífera Formation and seems to form a thrust slice between them.

The foliated metarhyolites have been studied in the Cordillera Riesco area, in the southeastern corner (Galaz, 2005) and Fiordo Peel in the northern part of the area covered by Figure 1. SHRIMP U-Pb dating of zircons in the metarhyolites have yielded an age of ca 152 Ma (unpubl. data) in the northern part of Fiordo Peel, and ages of ca.148 Ma in areas further south in both thrust slices (Calderón *et al.*, in press).

These rocks are intruded by granitic plutons at Fiordo Peel. A leucocratic foliated granite with miarolitic cavities 15 km south in Fiordo Peel showed a ca 150 Ma U-Pb zircon age (unpubl. data). Contrarily, other granites in the surroundings have U-Pb zircon ages of 18.8 Ma (see Fig. 1), and of ca. 20 Ma (Fanning *et al.*, 2001).

The strong foliation in the metarhyolites is roughly NS with dips of 45 to 85° W except in the northernmost outcrops where the NS foliation dips 66°E, with a lineation 50°SE. At Cordillera Riesco, the rocks of the Tobífera Formation bear evidence of a mylonitic foliation, and the kinematic indicators (strain fringes, quarter mats, S-C relations) indicate eastward thrusting with a dextral component. The foliation in the rhyolites is parallel to the one developed in the early Cretaceous pelites of the Erezcano formation in the SE corner of the map in Figure 1, as well as to the thrust plane separating the units. The foliated metarhyolites of the Tobífera Formation are cut by a basic dyke swarm which trends normal to the main foliation and is not affected by the deformation. Lamprophyre dykes which are part of this swarm are bracketed in time between 126 and 104 Ma (Calderón, 2006).

Given these observations, and although no direct determination of its age is available, the development of the mylonitic foliation and the metamorphism of the rhyolites probably took place during the thrusting of the Sarmiento ophiolite and the Tobífera Formation to the east during a late Neocomian compressional event (Dalziel, 1986; Fildani *et al.*, 2005).

3. Petrography

The metarhyolites at Fiordo Peel display a strong penetrative mylonitic foliation at the outcrop scale, which is not homogeneously developed throughout the whole unit. The presence of abundant quartz porphyroclasts up to 1 cm in diameter is conspicuous as well as the frequent occurrence of quartz veins, some of which are parallel to the foliation. Well developed strain shadows and quarter mats are observed around the porphyroclasts indicating top to the east displacement. The matrix is very fine grained. In some outcrops breccia and fiamme structures are preserved pointing to the presence of pyroclastic rocks in the succession.

Two samples of metarhyolitic rocks from the Fiordo Peel area were studied in detail. Sample FO0016 is composed of mm-sized subautomorphic quartz porphyroclasts, sericitized plagioclase, and spindle shaped bodies of fine grained aggregates of phyllosilicates, representing either former glass fragments or feldspar pseudomorphs, embedded in a fine grained matrix. These rock features can be attributed to an ignimbrite structure. The rock is penetratively foliated with the foliation mainly defined by oriented white mica and elongated trails of epidote. The strain shadows around the quartz porphyroclasts are composed of calcite, K-feldspar, white mica and quartz in fibers up to 0.1 by 0.01 mm elongated parallel to the foliation (Fig. 2). The minerals of the matrix are less than 30 microns in size and consist of a rather isotropic intergrowth of K-feldspar, albite, quartz, white mica, chlorite, epidote, allanite, calcite, with accessory stilpnomelane, biotite, pyrrhotite/pyrite, sphalerite, apatite, zircon, and

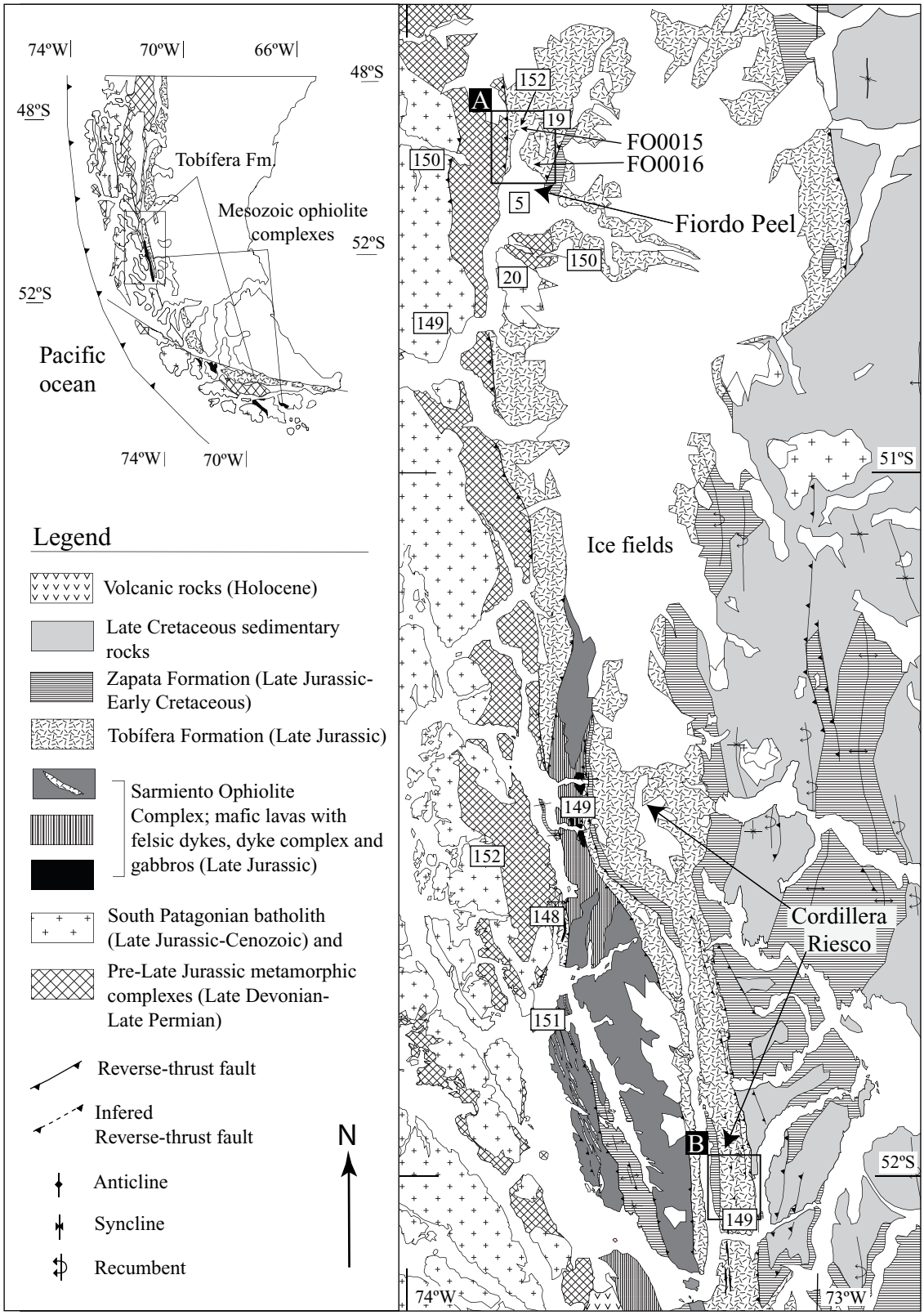

Fig. 1.- Geological sketch map of the area of occurrence of the foliated silicic metavolcanic Tobífera Formation . Area A is the one where the samples anlaysed in this paper come from. Area B is the area studied by Galaz (2005). Boxes indicate age in Ma obtained by SHRIMP U-Pb method in zircons interpreted as crystallization ages.

Fig.1.- Mapa geológico esquemático del área de afloramientos de la Formación Tobífera, compuesta principalmente por volcanitas silíceas foliadas. Área A es aquella de donde provienen las muestras analizadas en este studio. Área B es aquella estudiada por Galaz (2005). Los cuadros indican edades U-Pb en circones obtenidas utilizando el SHRIMP, y que son interpretadas como edades de cristalización.

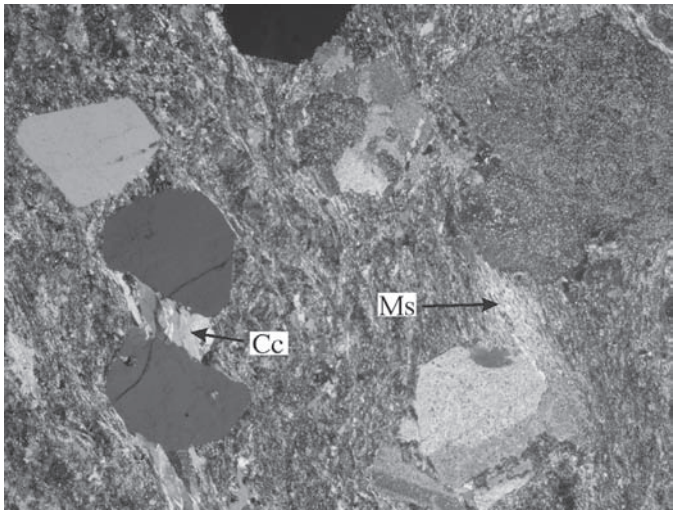

Fig. 2.- Foliated metarhyolite FO0016, showing quartz and albite porphyroclasts in a foliated fine grained matrix. Fibers in strain fringes between quartz are composed of carbonate and quarter mats associated to albite are composed of phengite. Optical microscope image, crossed polars. Width of figure is 2 mm.

Fig. 2.- Metariolita foliada FO0016, mostrando porfiroclastos de albita en una matriz foliada de grano fino. Las fibras en las sombras de presión entre cristales de cuarzo están compuestas de carbonato, y los "quarter mats" asociado a la albita están compuestos de fengita. Imagen al microscopio óptico, luz polarizada y analizada. El ancho de la figura es de 2 mm.

ilmenite decomposed to titanite and rutile. Except allanite, ilmenite and pyrrhotite which are probably of igneous origin, this mineral assemblage seems to have reequilibrated during the metamorphic episode.

Sample FO0015 also from Fiordo Peel, is probably of subvolcanic origin. The foliation is mainly defined by white mica, and by K-feldspar, calcite and quartz fibers in the strain shadows of the quartz and feldspar porphyroclasts. In addition to white mica, the matrix consists of K-feldspar, albite, and quartz with less opaque minerals than in FO0016. A grain of chlorite has been proven by electron microprobe as inclusion in K-feldspar.

4. Mineral Chemistry

4.1 Methods

The above samples were studied carefully first under the polarizing microscope and subsequently with a CAMECA SX100 electron microprobe (EMP) with 5 wavelength-dispersive spectrometers. The energy-dispersive system (EDS) of the EMP served as means of identification of phases during the selection of spots for full analyses. Moreover, we intensively used back-scattered electron (BSE) images for spot selection. We determined the concentrations of F, Na, Mg, Al, Si, K, Ca, Ti, Mn, Fe, Ba. Counting times were 20 s at the peak and on the background positions. To verify mineral compositions critical for the geothermobarometric evaluation, additional analyses were undertaken but without F and Ba. We used synthetic components (MgO for Mg) and natural minerals (orthoclase for Si and K, albite for Na, hematite for Fe, diopside for Ca and Mg, fluorite for F, rhodonite for Mn), as standards. The applied acceleration voltage and electric current were 15 kV and 15 nA, respectively. Beam diameter was about 5 μm but also 2 μm in case of small minerals. The PaP correction procedure provided by CAMECA was applied. Concentration maps for major elements (number of simultaneously prepared maps according to the number of WDS) were prepared by stepwise moving of the thin section under the electron beam of the probe and subsequent computer aided evaluation. Counting times per step were 100 or 200 ms.

4.2 Analytical results

Chemical analyses of the minerals in the studied samples are presented in Table 1. The minerals in the strain shadows, which are unequivocally syntectonic to the deformation/metamorphic episode, are similar in composition to the minerals in the matrix, indicating that the whole mineral assemblage was equilibrated during metamorphism. Nevertheless, a significant compositional variation was noted for several minerals in sample FO0016.

Potassic white mica: White mica analyses in sample FO0015 after calculation of the structural formula (double formula unit = d.f.u.) scatter around 6.47 Si/d.f.u. (Fig. 3). Only one analysis gave a significantly lower Si (6.27/d.f.u.) and Fe content. Na and Ti contents are generally low as typical for low-temperature metamorphic white micas. In sample FO0016 white micas show a stronger compositional variation (Fig. 4). In addition to a cluster again around 6.47 Si/d.f.u., potassic white micas appear which are clearly richer (~6.9/d.f.u.) and poorer in Si (6.2/d.f.u.). Referring to the mica group around 6.47 Si/d.f.u. its Mg and total Fe contents are about 0.6 and 0.7/d.f.u., respectively, in sample FO0016 but only 0.3 Mg and 0.5 Fe_{tot}/d.f.u. in sample FO0015. This discrepancy is explained by significant Fe^{3+} contents (ferrimuscovite component: $KAl_2Fe^{3+}Si_3O_{10}(OH)_2$) in white mica of sample FO0016. In order to estimate these contents, the octahedral occupancy of potassic white mica was fixed to 4.10/d.f.u. following a suggestion by Massonne (1995a). Values around 0.5 Fe^{3+}/d.f.u. (~ 25% ferrimuscovite component, see Table 1) result. However, a trend of decreasing Fe^{3+} contents with rising Si/d.f.u. is clearly discernable. Moreover, slightly decreasing Mg and increasing Na contents are related to increasing Si contents. For the low-Si white micas, negative Fe^{2+} contents result from

the calculation with an octahedral occupancy of 4.10/ d.f.u. This might indicate that the octahedral occupancy is actually higher at least for the low-Si white micas. This is confirmed by the experimental work of Massonne and Schreyer (1986) who reported increasing octahedral occupancies with decreasing Si contents as low as 6.2/d.f.u. at fixed P-T conditions. In order to better detect the distribution of the variable mica compositions, we scanned areas with abundant micas to produce element concentration maps. However, we could only detect moderate zonation in discrete mica grains. Thus, it could not be disproved that the wide chemical variability of potassic white mica in sample FO0016 is due to local variations (thin section range) in rock composition.

Chlorite: In sample FO0015, chlorite appears exclusively as rare inclusion in K-feldspar. The corresponding chlorite composition is given in Table 1 (Si ~ 5.8/d.f.u., X_{Mg} ~ 0.45). In contrast, chlorite is a common mineral in FO0016, where it shows a slight compositional variability (Fig. 5). Si contents and X_{Mg} vary between 5.4 to 5.8/d.f.u. and 0.41 to 0.44, respectively. A slight decrease of Fe with rising Si is discernable. In contrast to FO0015, we observed significant Mn contents (~0.12/d.f.u.) in chlorite of FO0016. The occurrence of chlorite associated to white mica is shown in Figure 6a.

Feldspars: Plagioclase in both samples is almost pure albite as typical for low-temperature metamorphic rocks. However, plagioclase with almost 8 mol% anorthite component determined by a spot analysis on FO0016 could be either due to a relic composition of magmatic plagioclase or, more likely as the K_2O content is very low, an indication of elevated metamorphic temperatures. K-feldspar compositions in FO0016 contain less than 6 mol% of components other than $KAlSi_3O_8$. In FO0015 these components can amount to almost 8 mol% but, in contrast to FO0016, the Ba end-member $BaAl_2Si_2O_6$ can reach almost 4 mol%.

Stilpnomelane and biotite: K-bearing phases other than white mica and K-feldspar were only observed in FO0016. Stilpnomelane typically forms intergrown aggregates (see figure 6 b). The chemical composition of stilpnomelane is somewhat variable especially in regard of alkalies (Fig. 7). As the sum of K + Na (+ very minor Ca+Ba) can reach 9/f.u. and thus values significantly above that of the maximum interlayer site (= 5/f.u.), it is assumed that alkalies are also introduced in the H_2O bearing layer between the tetrahedral layers of the stilpnomelane structure. X_{Mg} of stilpnomelane is around 0.23. Biotite is significantly richer in Mg (X_{Mg} ~ 0.45) as typical for biotite + stilpnomelane-bearing assemblages (e.g., Brown, 1975).

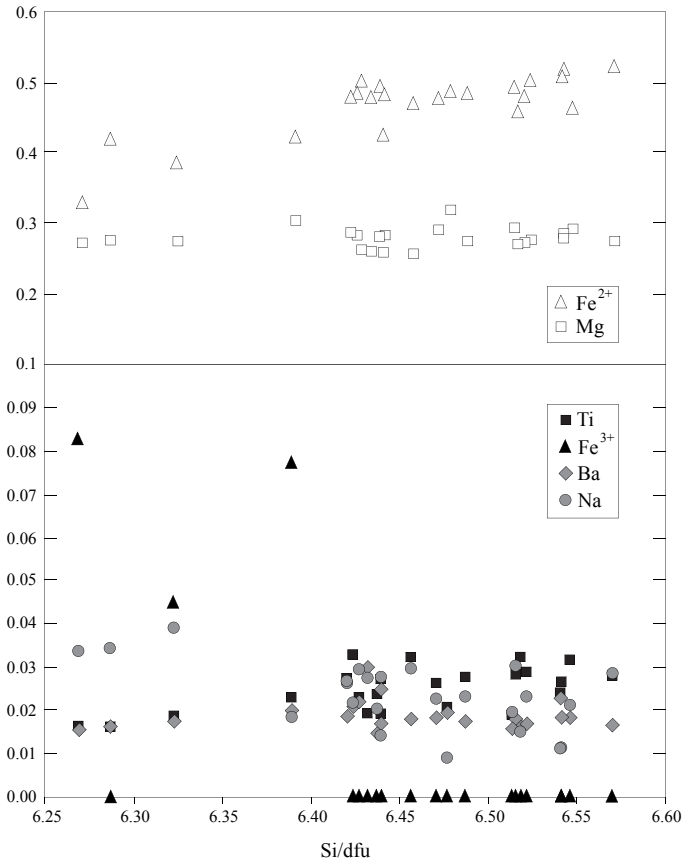

Fig. 3.- Chemical composition of white mica in sample FO0015. Cation contents per double formula unit (d.f.u)

Fig. 3.- Composición química de mica blanca en la muestra FO0015. El contenido de cationes se expresa en número por doble fórmula unidad (d.f.u)

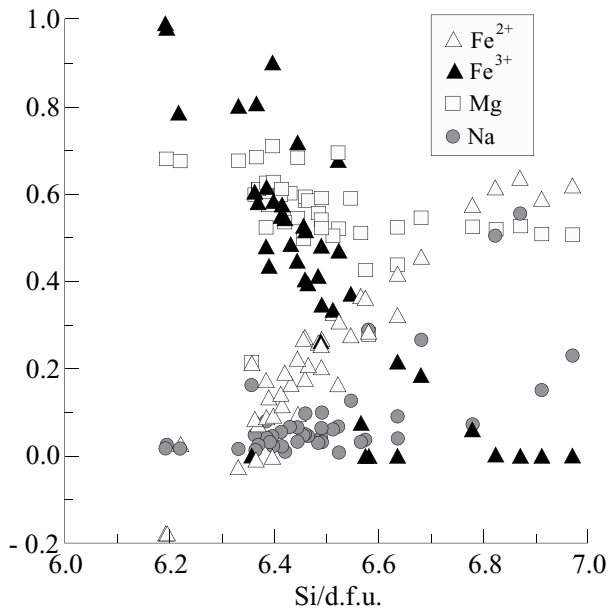

Fig. 4.- Chemical composition of white mica in sample FO0016. Note increase in Na and decrease in Mg with higher Si content per double formula unit (d.f.u.).

Fig.4.- Composición química de mica blanca en la muestra FO0016. Destaca el aumento de Na y la disminución de Mg con mayor contenido de Si por doble fórmula unidad (d.f.u)

Mineral	**Muscovite-Phengite (O = 24)**								**Chlorite (O = 36)**				**Stilpnomelane (O = 192)**		**Biotite (O = 12)**	**Feldspars (O = 8)**						**Titanite (Si = 1)**	
Sample No.	*FO-0016*				*FO-0015*				*FO-0016*			*FO-0015*	*FO-0016*		*FO-0016*	*FO-0016*			*FO-0015*				*FO-0016*	
Anal. No.	*24.15*	*30.44*	*18.21*	*18.20*	*24.1*	*24.19*	*24.21*		*30.39*	*18.23*	*18.26*	*1.15*	*30.49*	*30.42*	*25.3*	*18.18*	*30.15*	*18.16*	*1.10*	*24.14*	*1.5*	*18.14*	*18.10*
SiO2 (wt.%)	46.13	46.94	48.54	50.83	48.22	47.47	46.38		25.02	26.61	25.87	26.83	46.00	46.46	36.31	64.08	65.93	66.75	62.86	63.66	68.74	31.11	30.22
TiO2	0.13	0.05	0.07	0.05	0.27	0.19	0.16		0.04	0.01	0.03	0.03	0.02	0.02	0.90	0.01	0.03	0.03	0.03	0.02	0.01	28.86	36.36
Al2O3	27.72	26.78	26.00	25.23	29.08	30.50	32.21		19.30	18.52	18.32	17.69	6.35	6.29	17.31	18.38	20.77	19.78	18.56	18.58	20.02	7.53	1.75
FeO	7.16	6.01	5.57	5.18	4.57	4.23	3.62		30.05	29.80	29.84	29.45	31.09	29.85	20.36	0.11	0.05	0.14	0.00	0.01	0.01	0.84	1.21
MnO	0.17	0.05	0.06	0.07	0.01	0.01	0.00		0.83	0.58	0.62	0.16	1.07	1.58	0.32	0.00	0.04	0.00	0.02	0.00	0.02	0.00	0.04
MgO	3.41	2.90	2.67	2.51	1.37	1.41	1.37		12.20	12.85	12.87	13.62	5.42	5.37	9.12	0.01	0.00	0.02	0.00	0.00	0.01	0.20	0.04
CaO	0.01	0.01	0.07	0.05	0.00	0.02	0.00						0.00	0.03	0.02	0.00	1.53	0.31	0.00	0.00	0.24	28.54	28.79
Na2O	0.10	0.19	1.00	0.57	0.11	0.05	0.13						0.66	1.43	0.20	0.52	10.38	11.57	0.41	0.38	11.76	0.09	0.00
K2O	10.72	10.88	9.82	9.86	10.76	10.59	10.98						1.89	1.84	9.47	15.72	0.10	0.20	15.49	15.56	0.36	0.21	0.03
BaO	0.28	0.20	0.25	0.23	0.31	0.47	0.29						0.06	0.06	n.d.	0.82	0.02	0.04	2.13	0.46	0.10		
Total	95.83	94.01	94.04	94.58	94.69	94.95	95.13		87.45	88.37	87.54	87.78	92.56	92.93	93.99	99.64	98.84	98.82	99.50	98.68	101.27	97.38	98.43
F	0.00	0.00	0.08	0.07	0.00	0.00	0.00			0.06	0.17		n.d.	0.19	n.d.							2.20	0.81
Si	6.225	6.459	6.680	6.911	6.570	6.440	6.284		5.462	5.708	5.623	5.776	63.04	63.27	2.819	2.986	2.922	2.960	2.963	2.984	2.975	1.000	1.000
Alt	1.775	1.541	1.320	1.089	1.430	1.560	1.716		2.538	2.292	2.377	2.224	8.96	8.73	1.181	1.010	1.085	1.034	1.031	1.026	1.021		
sum	8.000	8.000	8.000	8.000	8.000	8.000	8.000		8.000	8.000	8.000	8.000	72.00	72.00	4.000								
Alo	2.634	2.802	2.897	2.952	3.240	3.316	3.426		2.429	2.389	2.314	2.266	1.29	1.36	0.052							0.285	0.068
Ti	0.013	0.005	0.007	0.005	0.028	0.019	0.016		0.007	0.002	0.005	0.004	0.02	0.02	0.402	0.000	0.001	0.001	0.001	0.001	0.000	0.698	0.905
Fe2	0.030	0.176	0.456	0.589	0.520	0.480	0.410		5.486	5.345	5.424	5.302	35.64	34.00	1.322								
Fe3	0.779	0.516	0.185	0.000	0.000	0.000	0.000									0.004	0.002	0.005	0.000	0.001	0.000	0.023	0.033
Mn	0.020	0.006	0.007	0.007	0.002	0.001	0.000		0.154	0.105	0.114	0.030	1.24	1.83	0.021	0.000	0.001	0.000	0.001	0.000	0.001	0.000	0.001
Mg	0.685	0.594	0.547	0.509	0.277	0.286	0.276		3.971	4.109	4.168	4.373	11.08	10.91	1.055	0.000	0.000	0.001	0.000	0.000	0.001		
sum	4.160	4.100	4.100	4.063	4.067	4.103	4.128		12.047	11.950	12.026	11.975	49.26	48.12	2.852	4.001	4.011	4.001	3.996	4.011	3.998	1.006	1.007
Ca	0.002	0.001	0.010	0.007	0.000	0.003	0.001						0.00	0.04	0.001	0.000	0.073	0.014	0.000	0.000	0.011	0.983	1.021
Ba	0.015	0.011	0.013	0.012	0.017	0.025	0.016						0.03	0.03		0.015	0.000	0.001	0.039	0.008	0.002		
Na	0.025	0.050	0.267	0.151	0.029	0.014	0.034						1.74	3.77	0.030	0.047	0.892	0.995	0.037	0.034	0.987	0.006	0.000
K	1.846	1.910	1.725	1.711	1.870	1.833	1.897						3.31	3.19	0.938	0.934	0.006	0.011	0.932	0.930	0.020		
sum	1.888	1.972	2.014	1.881	1.916	1.875	1.947						5.08	7.03	0.969	0.997	0.971	1.021	1.008	0.973	1.019	0.989	1.021
F	0.00	0.00	0.03	0.03	0.00	0.00	0.00			0.04	0.12											0.22	0.09
H	4.00	4.00	3.96	3.97	4.00	4.00	4.00		16.00	15.96	15.88	16.00			2.00								
Xms	0.5754	0.5513	0.4047	0.4097	0.6348	0.6822	0.7517	xSi	0.6828	0.7135	0.7028	0.7220			Xan+cs	0.0152	0.0752	0.0148	0.0390	0.0087	0.0127		
X(trioctah. comp.)	0.0800	0.0500	0.0500	0.0316	0.0335	0.0514	0.0642	xMg	0.4131	0.4298	0.4294	0.4506			Xab	0.0473	0.9188	0.9742	0.0370	0.0354	0.9678		
XMg-Al-Cel	0.1162	0.1818	0.1917	0.2157	0.1022	0.0876	0.0605	xFe	0.5708	0.5591	0.5588	0.5463			Xkf	0.9375	0.0059	0.0110	0.9240	0.9559	0.0195		
XFe-Al-Cel	0.0050	0.0539	0.1600	0.2497	0.1917	0.1470	0.0899																
Xparag	0.0133	0.0252	0.1323	0.0804	0.0149	0.0076	0.0173	acli	0.00826	0.01201	0.01126	0.01595											
X(other comp.)	0.2100	0.1379	0.0613	0.0128	0.0228	0.0243	0.0165																

Table 1. Representative analyses of minerals from metarhyolites of the Tobifera Formation

Tabla 1.- Análisis químicos representativos de los minerales de las metariolitas de la Formación Tobífera.

Titanite and other Ti-phases: Titanite, ilmenite, and rutile form large aggregates (leucoxene) demonstrating that these aggregates are alteration products of former magmatic minerals probably ilmenite. BSE images (Fig. 6 c,d) and observations under reflected light show that titanite has finally replaced rutile and ilmenite in these aggregates. According to our EDS analysis rutile and ilmenite (only minor Mn) are virtually pure phases. Therefore, our analytical work concentrated on titanite. For sample FO0016, we obtained very different chemical compositions that show variations in Ti between 0.6 and 0.9 Ti/f.u. Al and Fe, assumed to be trivalent, amount to 0.07 to almost 0.4/f.u. and 0.02 to 0.04/f.u., respectively. These trivalent cations are widely balanced by F (+OH) according to the substitution Me^{3+} + F (+OH) = Ti + O.

Other minerals: According to EDS analyses apatite, pyrrhotine, and pyrite are virtually pure phases. Epidote is frequent in the foliated matrix and occasionally formed around allanite that is probably of igneous origin.

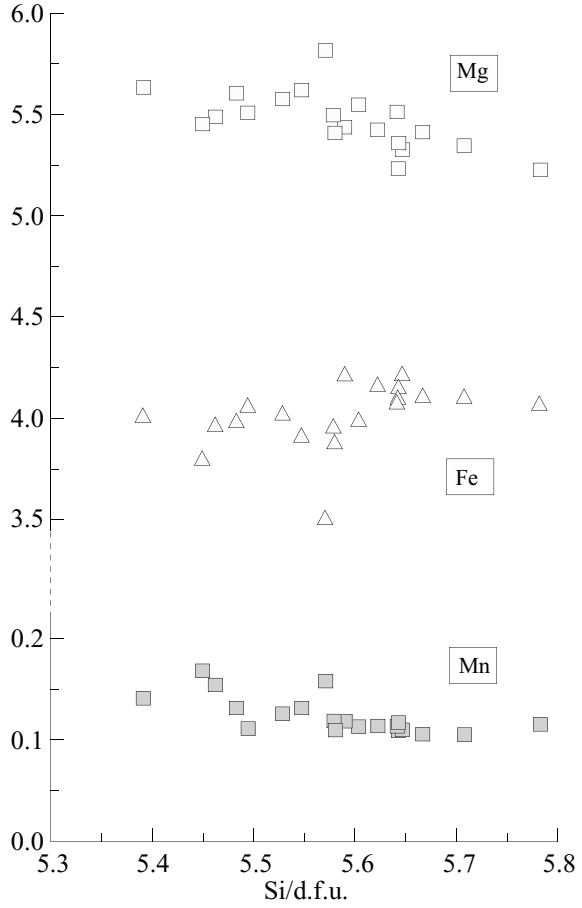

Fig. 5.- Chemical composition of chlorite in the analysed metarhyolitic rocks.

Fig. 5.- Composición química de clorita en las rocas metariolíticas analizadas.

5. Conditions of Metamorphism

Qualitatively, we can estimate a P-T range from the observed mineral assemblage. K-feldspar + chlorite is only stable at low metamorphic temperatures. For instance, Massonne (1995a) estimated maximum T around 330°C (P ~ 2 to 6 kbar) for the stability of this assemblage. This is widely confirmed by thermodynamic calculations of phase relations, for instance, in the system K_2O-FeO-Al_2O_3-SiO_2-H_2O by Massonne and Szpurka (1997). However the corresponding P-T curve (2 kbar, 350°C; 4 kbar, 310°C) of the reaction chlorite + K-feldspar = muscovite/phengite + biotite + quartz + H_2O is significantly curved (Fig.8). As small biotite crystals had already formed in sample FO0016, metamorphic temperatures around 330°C or somewhat higher might have been reached. Referring to this temperature, metamorphic pressures could have been elevated due to the assemblage phengite + stilpnomelane. Calculation results by Massonne and Szpurka (1997) point to minimum pressures of 4 kbar at T > 300°C (Fig. 8). However, as no jadeite was observed, maximum pressures of 10 kbar (~ 300°C) should be taken into account (Popp and Gilbert, 1972).

Furthermore, a trend of rising P and T conditions can be estimated from the observed compositional variation. Referring to potassic white mica and a constant, here relevant mineral assemblage, rising Si contents, which we prefer over decreasing Si contents, would point to increasing pressure. Rising Na contents indicate rising temperatures according to the known muscovite-paragonite solvus (e.g., Chatterjee and Flux, 1986) especially since higher Na contents were observed in Si richer micas. At constant P-T conditions, decreasing Na contents are generally observed with rising Si contents in natural muscovite/phengite + paragonite assemblages. Maximum pressures could already lie in the high-pressure metamorphic range as the Si contents in phengite (~6.9/d.f.u.) and the Al(+Fe^{3+}) contents in titanite (>0.4/f.u.) are high. In order to quantitatively define the relevant P-T conditions, we applied the subsequent geothermobarometers based on thermodynamic calculation methods.

5.1 Geothermobarometric methods

We applied two thermodynamic data sets (Massonne, 1992; Vidal *et al.*, 2001) which both are based on the data set by Berman (1988). Vidal *et al*. (2001) augmented Berman`s data by data for components of chlorite (amesite = $Mg_4Al_2[Al_2Si_2O_{10}](OH)_8$, daphnite = $Fe_5Al[AlSi_3O_{10}](OH)_8$) and potassic white mica (pyrophyllite = $Al_2[Si_4O_{10}](OH)_2$, Mg-Al-celadonite = $KAlMg[Si_4O_{10}](OH)_2$, Fe-Al-celadonite =

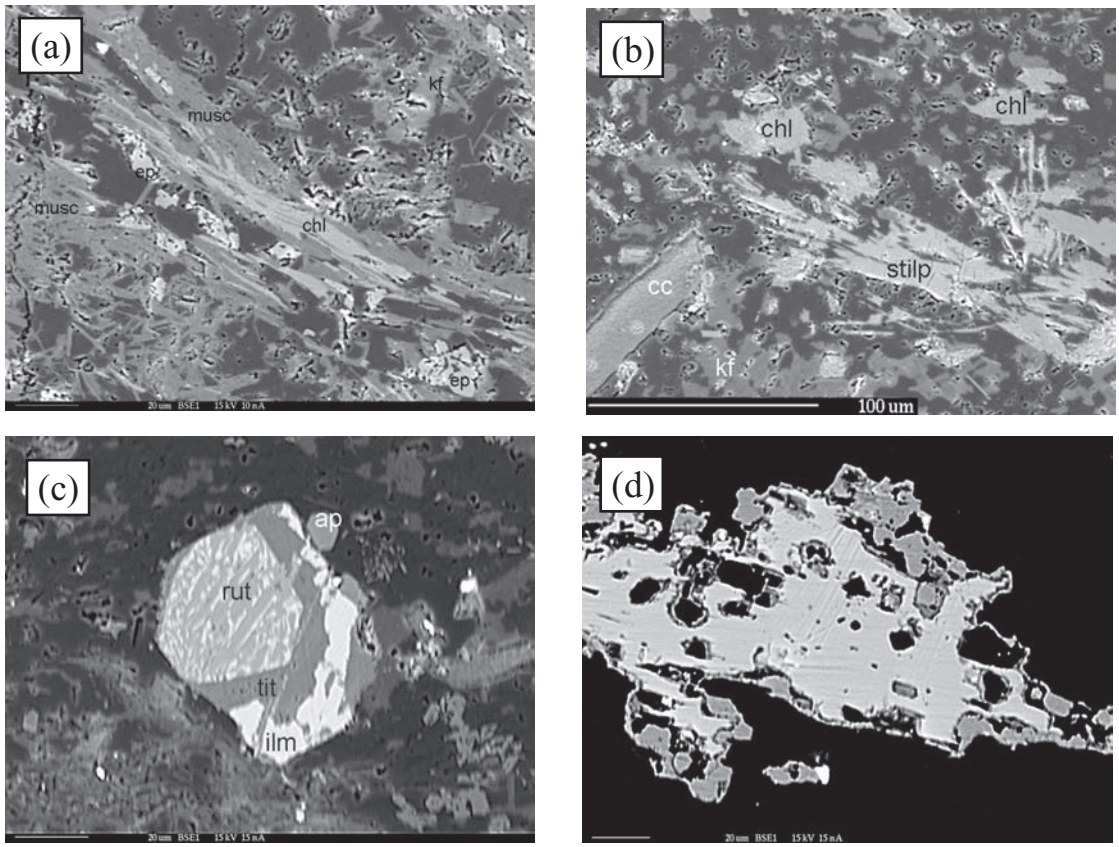

Fig. 6.- Characteristic mineralogy and texture of the analysed samples. a) Oriented phyllosilicates (white mica and chlorite) embedded in feldspar matrix with isolated epidote grains. b) Stilpnomelane crystals associated with chlorite, K-feldspar and quartz. An isolated calcite crystal is also shown. c) Textural relationships among Ti- rich phases ilmenite, titanite and rutile. An isolated apatite automorph is also present. d) a large ilmenite crystal with titanite corona.

Fig.6.- Mineralogía y textura características de las muestras analizadas. a) Filosilicatos (mica blanca y clorita) orientados, en matriz de feldespatos con granos aislados de epidota. B) Cristales de estilpnomelano asociados con clorita, feldespato potásico y cuarzo. Se observa también un cristal aislado de calcita. C) Relaciones texturales entre las fases ricas en titanio ilmenita, titanita y rutilo. Un cristal automorfo de apatita tambien está presente. d) Un cristal mayor de ilmenita con una corona de titanita.

$KAlFe[Si_4O_{10}](OH)_2$) and corresponding activity models for both phases. Thus, various equilibria (e.g., E1 and E2 given in Table 2) could be calculated for T values between 250ºC and 400ºC considering the above components, the clinochlore (= $Mg_5Al[AlSi_3O_{10}](OH)_8$) component in chlorite, the muscovite ($KAl_2[AlSi_3O_{10}](OH)_2$) component in potassic white mica as well as K-feldspar, quartz and H_2O. Further equilibria considering the Fe-Al-celadonite component were ignored because of the poorly defined content of this component according to the Fe^{2+}/Fe^{3+} estimation method applied to potassic white mica. This method has an almost negligible influence on the content of Mg-Al-celadonite. The data set by Massonne (1992) was applied because of thermodynamic data for Mg-Al-celadonite and the mixing properties of the potassic white mica solid solution series that was added to Berman`s data. With these data the P-T positions of equilibrium E3 (see Table 2) and, under consideration of biotite, invariant point IP1 (Table 2) were calculated. The computer programs PTAX (Brown *et al.*, 1988) and

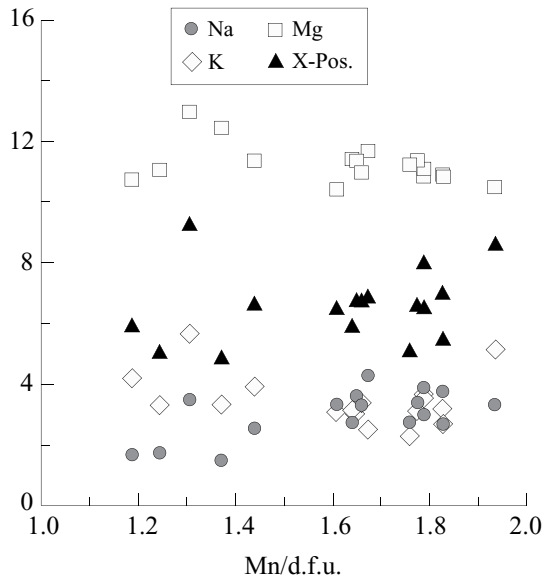

Fig. 7.- Chemical composition of stilpnomelane in sample FO0016. Numbers express cations per double formula unit (d.f.u.).

Fig. 7.- Composición química del estilpnomelano en la muestra FO0016. Los números expresan cationes por doble formula unidad (d.f.u).

Sample	Equilibrium	White Mica		Chlorite		P	T
		Anal. No.	Si/d.f.u.	Anal. No.	Si/d.f.u.	kbar	°C
FO0016	E3	24.15	6.23	30.39	5.46	3.2	250
						4.3	350
	E3	30.44	6.46	30.39	5.46	4.1	250
						5.4	350
	E3	18.21	6.68	18.26	5.62	5.5	250
						7.1	350
	E3	18.20	6.91	18.23	5.71	6.1	250
						7.7	350
	IP1 (aphl = 0.0870)					7.38	330
	IP1 (aphl = 0.0566)					6.90	301
	E4					8.0	350
						9.5	400
FO0015	E3	24.21	6.28	1.15	5.78	2.1	250
						3.0	350
	E3	24.19	6.44	1.15	5.78	3.5	250
						4.6	350
	E3	24.1	6.57	1.15	5.78	4.2	250
						5.5	350

Equilibria

E1	6 Mg-Al-celadonite + 1 amesite = 2 clinochlore + 6 K-feldspar + 2 quartz + 2 H2O
E2	4 Mg-Al-celadonite + 2 muscovite = 6 K-feldspar + 1 amesite + 2 quartz + 2 H2O
E3	5 Mg-Al-celadonite + 1 muscovite = 1 clinochlore + 6 K-feldspar + 2 quartz + 2 H2O
E4	3 Mg-Al-celadonite = 1 phlogopite + 2 K-feldspar + 3 quartz + 2 H2O
IP1	intersection of 6 equilibria with the subsequent participating mineral components: Mg-Al-celadonite, muscovite, phlogopite, clinochlore, K-feldspar, quartz, H2O

Table 2.- Examples of results of metamorphic pressures calculated using thermodynamic data.
Tabla 2.- Ejemplos de resultados de presiones metamórficas obtenidas mediante el uso de datos termodinámicos

PTGIBBS (Brandelik and Massonne, 2004) were applied for the thermodynamic computation. Simple activity relations were used for the clinochlore component in chlorite (Massonne, 1995a) and the phlogopite component in biotite (Massonne, 1995b) by applying Massonne´s data set. The activity of K-feldspar was set to 0.95 using both thermodynamic data sets. This choice is justified by K-feldspar compositions close to the end member (see Table 1).

5.2 P-T data

The calculated P-T positions of equilibria using the thermodynamic dataset by Vidal *et al.* (2001) showed a strong scatter when those with pyrophyllite component in potassic white mica and amesite component in chlorite (see equilibria 1 and 2) were considered. We think that this observation is due to thermodynamic data for these components which are not well defined. For this reason we abandoned the corresponding equilibria. However, thermobarometry with phengite (see, e.g., Massonne, 1995a) related to E3 gave consistent results. We observed an increase of P from almost 4 kbar to 7 kbar with rising Si content of the mica at 300°C (see Table 2). If we would additionally consider that Si-rich phengites formed at the highest T (close to 350°C), as argued above, and that the Si poorest micas were stable at the lowest T (presumably between 200 to 250°C = earliest stage) of the formation of the metarhyolites, the detectable P-T path would start at about 3 kbar (200-250°C) and end close to 7 kbar and 350°C. This pressure was confirmed by the consideration of the phlogopite component in biotite and, thus, the possibility to calculate IP1. For the phlogopite activity calculated according to Massonne (1995b) a P-T date of 6.9 kbar and 301°C resulted. However, assuming a higher activity coefficient γ instead of 1.3 (resulting in a_{phl} = 0.0566 for the biotite analysis in Table 1), as it is likely for the low temperature conditions, a somewhat higher P-T date results (7.4 kbar, 330°C for γ = 2.0 and, thus, a_{phl} = 0.087). Among the reaction curves intersecting in IP1 there is one which is independent of water activity. The other reactions curves such as E1 to E4 are dependent on

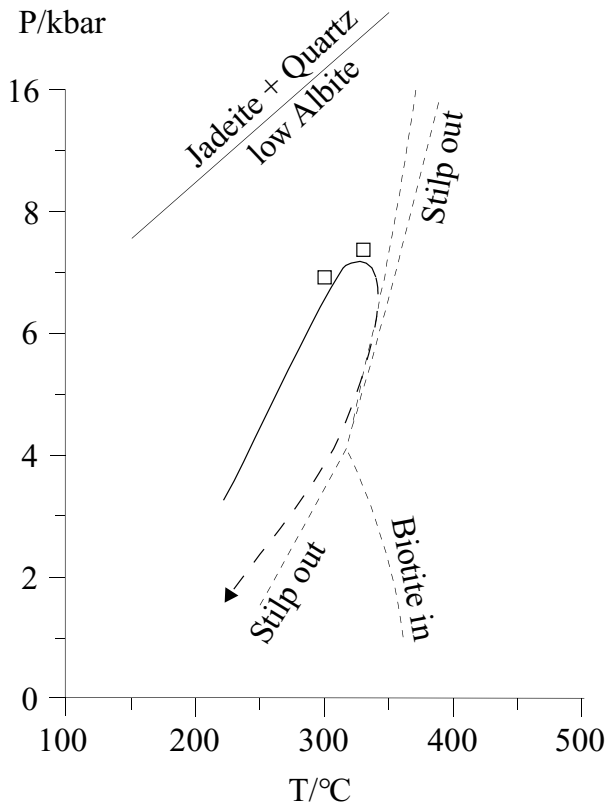

Fig. 8 .- P-T path for the metamorphism of the Tobífera Formation rhyolitic rocks at Fiordo Peel derived by phengite thermobarometry using thermodynamic calculation methods.

Fig.8.- Trayectoria P-T del metamorfismo de las rocas riolíticas de la Formación Tobífera en Fiordo Peel derivados de la termobarometría de fengita usando métodos de cálculo termodinámico.

this parameter, which was set to unity for the above calculations. A reduced water activity would result in (somewhat) higher pressures.

Considering these discussed P-T uncertainties, we believe that the P-T conditions for the metamorphic peak are 7.4 kbar and 330°C with an estimated 2 sigma accuracy of ± 1 kbar and ± 30 °C. The magnitude of these errors result from the aforementioned P-T restrictions and also our experience with the derivation of P-T paths for similar rocks investigated along the Coastal Cordillera of Chile (Massonne *et al.*, 1996; Willner *et al.*, 2000, 2004).

6. Discussion and conclusions

The uncertainties of the P-T data are related to the variability of mineral compositions within the studied rocks and to the lack of control of thermodynamic parameters, such as water activity, effective during the metamorphic processes. However, a general trend toward rather high metamorphic pressures at low temperatures of metamorphism is clearly shown by the observed mineral associations. The P-T path derived by phengite thermobarometry (Fig. 8) using thermodynamic calculation methods is at least compatible with the mineral assemblages found. Thus, we take it here as the most probable metamorphic conditions in which the metamorphism of the metarhyolites evolved.

These results are also comparable to the values assigned to peak metamorphic conditions obtained by Galaz (2005)and Galaz *et al*. (2005) (399 +- 64 ºC and 6.37 +- 1.1 kb) for mylonitic rocks of the Tobífera Formation at Cordillera Riesco using the Currie and Van Staal (1999) geothermobarometer. These values suggest that the Tobífera formation was regionally affected by this rather high pressure and low temperature metamorphism. Massonne *et al* (2004) indicate that muscovite-garnet-bearing granites, probably also 150 Ma in age, were emplaced at a depth corresponding to 5.5 kbar, the same range indicated by the metamorphic minerals in the studied rhyolites, an indication of the magnitude of the regional exhumation of these rock bodies.

Although as yet there is no dating of the phases formed during the metamorphic event registered in the metarhyolites, the syntectonic nature of the minerals strongly suggests that the metamorphism took place during the initial thrusting of the rocks during an early compressional phase which took place during the Early to middle Cretaceous. This implies that the rhyolites, were buried to 10 km and then to somewhat more than 20 km depth sometimes between 150 and 100 Ma, contemporaneously to the construction of a large portion of the South Patagonian Batholith and of the Sarmiento ophiolite. This scenario is shown in Figure 9, together with a cross section of the present relationships between the involved units. Kraemer (2003) had already pointed out that restoration of the observed maximum shortening of the Patagonian Andes south of the area referred to in this paper needs that the back arc oceanic lithosphere represented in the study area by the Sarmiento ophiolite was partially consumed during a short episode of reverse subduction during the mid-Cretaceous compressive event. The metamorphism revealed in this study might have been developed during this episode of subduction.

The emplacement of the early Miocene plutons appears to be unrelated to the observed metamorphism.

Acknowledgements

Field work was supported by Fondecyt Project 1010412 and 1050431 to FH. Laboratory work was undertaken at Universität Stuttgart under the BMBF – CONICYT

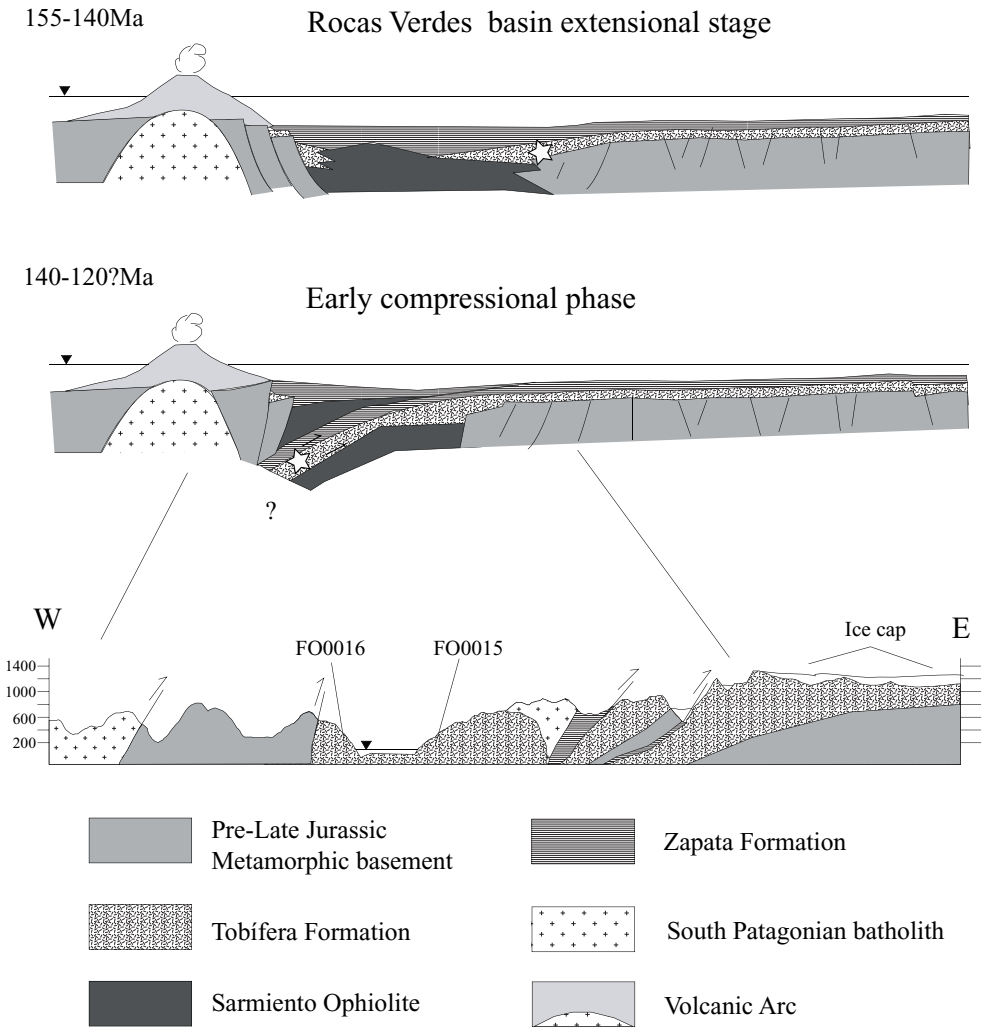

Fig. 9.- Schematic reconstructions of the environment of deposition (155 – 140 Ma) and metamorphism (140-120? Ma) of the Tobífera Formation, together with an EW cross section of the present geology of the studied area. Star indicates the possible location of the studied rocks during their deposition and metamorphism.

Fig. 9.- Reconstrucciones esquemáticas de los ambientes de deposición (155 a 140 Ma) y metamorfismo (140 – 120? Ma) de la Formación Tobífera, junto a una sección EW de la geología actual del área estudiada. La estrella indica la posible posición de las rocas estudiadas durante su deposición y metamorfismo.

Project 20026238 to H-J. M and F.H. The manuscript greatly benefited from thorough reviews by Drs. César Casquet and Ricardo Arenas. Captain Conrado Alvarez and his crew took us safely in the yacht Penguin to these remote areas.

References

Berman, R.G. (1988): Internally-consistent thermodynamic data for minerals in the system Na_2O-K_2O-CaO-MgO-FeO-Fe_2O_3-Al_2O_3-SiO_2-TiO_2-H_2O-CO_2. *Journal of Petrology*, 29: 445-522.

Brandelik, A., Massonne, H.-J. (2004): PTGIBBS - an EXCEL™ Visual Basic program for computing and visualizing thermodynamic functions and equilibria of rock-forming minerals. *Computers and Geosciences*, 30, 908 - 923.

Brown, T.H., Berman, R.G., Perkins, E.H. (1988): Ge0-Calc: Software package for calculation and display of pressure-temperature-composition phase diagrams using an IBM or compatible Personal Computer. *Computes and Geoscience,* 14: 279-289.

Calderón, M. (2006): *Petrogenesis and tectonic evolution of Late Jurassic bimodal magmatic suites (Sarmiento Complex) and migmatites (Puerto Edén Igneous Metamorphic Complex) in the southern Patagonian Andes, Chile.* PhD Thesis, Universidad de Chile, 178 p., Santiago.

Calderón ,M., Fildani, A., Hervé, F., Fanning, C.M., Weislogel, A., Cordani, U (2007, in press): Late Jurassic bimodal magmatism in the northern seafloor remnant of the Rocas Verdes basin, southern Patagonian Andes. *Journal of the Geological Society of London.*

Currie, K.L., Van Staal, C. R. (1999): The assemblage stilpnomelane – chlorite – phengitic mica : a geothermobarometer for blueschist and associated greenschist terranes. *Journal of Metamorphic Geology*, 17: 613 – 620.

Chatterjee, N.D., Flux, S. (1986): Thermodynamic mixing properties of muscovite - paragonite crystalline solutionsat high temperatures and pressures, and their geological application. *Journal of Petrology*, 27: 677-693.

Dalziel, I.W.D. (1986): Collision and cordilleran orogenesis: An Andean perspective. In: Coward, M.P. and Ries, A.C. (eds) Collision tectonics. *Geological Society Special Publication* 19: 389–404.

Fanning, C.M., Hervé, F., Pankhurst, R.J., Thomson, S., Faúndez, V. (2001): Late Cenozoic magmatism in the South Patagonian batholith: SHRIMP U-Pb zircon age evidence. *Expanded Abstracts Volume, III Southamerican Symposium of Isotope Geology*, Pucón, Chile: pp. 30-33.

Fildani, A., Cope, T., Graham, S.A., Wooden, J. (2003): Initiation of the Magallanes foreland basin: timing of the southernmost Patagonian Andes orogeny revised by detrital zircon provenance analysis. *Geology*, 31 (12): 1081-1084.

Fildani, A., Hessler, A.M. (2005): Stratigraphic record across a retroarc basin inversion: Rocas Verdes-Magallanes basin, Patagonian Andes, Chile. *Geological Society of America Bulletin,* 117, 11/12, 1596-1614.

Galaz, G. (2005): *Petrología de la Formación Tobífera en Cordillera Riesco, Region de Magallanes, Chile*. Graduation Thesis, Universidad de Chile, 127 pp.

Galaz, G., Hervé, F., Calderón, M.. (2005): Metamorfismo y deformación de la Formación Tobífera en la Cordillera Riesco, Región de Magallanes, Chile. *Revista de la Asociación Geológica Argentina,* 60, 4: 762-774.

Kraemer, P. E. (2003): Orogenic shortening of the Patagonian orocline (56^0 S. Lat). *Journal of South American Earth Sciences*, 15: 731-748.

Massonne, H.-J. (1992): Thermochemical determination of water activities relevant to eclogitic rocks. In: Kharaka, Y.K. and Maest, A. (eds.): *Water-rock interaction WRI-7*, Proc. 7th Int. Symp., Park City, Utah, U.S.A., 2: 1523-1526.

Massonne, H.-J. (1995a): III. Rhenohercynian Foldbelt, C. Metamorphic units (Northern phyllite zone), 4. Metamorphic evolution. In: Dallmeyer, R.D., Franke, W. and Weber, K. (eds.): *Pre-Permian geology of central and eastern Europe*. Berlin: Springer Verlag: 132-137.

Massonne, H.-J. (1995b): Is the concept of 'in situ' metamorphism applicable to deeply buried continental crust with lenses of eclogites and garnet peridotites? *Chinese Science Bulletin Supplement*, 40: 145-147.

Massonne, H.-J., Schreyer, W. (1986): High-pressure syntheses and X-ray properties of white micas in the system K_2O-MgO-Al_2O_3-SiO_2-H_2O. *Neues Jahrbuch Mineralogie Abhandung*, 153: 177-215.

Massone, H-J., Szpurka,Z. (1997): Thermodynamic properties of white micas on the basis of high pressure experiments in the systems $K_2$0-MgO-Al_2O_3-SiO_2-H_2O and K_2O-FeO-Al_2O_3-SiO_2-H_2O. *Lithos*, 41: 229-250.

Massonne, H.-J., Hervé, F., Muñoz, V., Willner, A.P. (1996): New petrological results on high-pressure, low-temperature metamorphism of the Upper Palaeozoic basement of Central Chile. *3éme Symposium International sur la Géodynamique Andine*, Saint-Malo (France), Extended Abstracts: 783-785.

Massone, H-J, Calderón, M., Hervé, F. (2004): Magmatic muscovite and garnet in granites of the southern Patagonian batholith. In: Extended Abstracts, GEOSUR International Symposium on the Geology and Geophysics of the Southernmost Andes, the Scotia Arc and the Antarctic Peninsula, J. Carcione, F.Donda, E.Lodolo Guest editors, *Bolletino di Geofísica Teorica ed Applicata*, 45: 121-125.

Pankhurst, R.J., Rapela, C.W. (1995): Production of Jurassic rhyolite by anatexis of the lower crust of Patagonia. *Earth and Planetary Science Letters*, 134: 23 – 36.

Popp R.K., Gilbert, M.C. (1972): Stability of acmite-jadeite pyroxenes at low pressure. *American Mineralogist*, 57: 1210-1231.

Vidal, O., Parra, T., Trotet, F. (2001): A thermodynamic model for Fe-Mg aluminous chlorite using data from phase equilibrium experiments and natural pelitic assemblages in the 100° to 600°C, 1 to 25 kb range. *American Journal of Science*, 301: 557-592.

Willner, A.P., Hervé, F., Massonne, H.-J. (2000): Mineral chemistry and pressure-temperature evolution of two contrasting high-pressure low-temperature belts in the Chonos Archipelago, Southern Chile. *Journal of Petrology*, 41: 309-330.

Willner, A.P., Thomson, S.N., Hervé, F., Massonne, H.-J., (2004). Converging PT paths of different HP-LT metamorphic units within a Mesozoic accretionary belt (Diego de Almagro Island / Chile): Evidence for juxtaposition during late shortening of an active continental margin. *Mineralogy and Petrology*, 81: 43-84.